Self-Assembly of Focal Point Oligo-catechol Ethylene Glycol Dendrons on Titanium Oxide Surfaces: Adsorption Kinetics, Surface Characterization, and Nonfouling Properties

ARTICLE *in* JOURNAL OF THE AMERICAN CHEMICAL SOCIETY · JUNE 2011

Impact Factor: 12.11 · DOI: 10.1021/ja202760x · Source: PubMed

8 AUTHORS, INCLUDING:

Edmondo M Benetti
ETH Zurich
35 PUBLICATIONS **566** CITATIONS
SEE PROFILE

Wen li
Shanghai University
37 PUBLICATIONS **730** CITATIONS
SEE PROFILE

Afang Zhang
Shanghai University
77 PUBLICATIONS **1,579** CITATIONS
SEE PROFILE

Marcus Textor
ETH Zurich
331 PUBLICATIONS **13,989** CITATIONS
SEE PROFILE

JACS
JOURNAL OF THE AMERICAN CHEMICAL SOCIETY

ARTICLE

pubs.acs.org/JACS

Self-Assembly of Focal Point Oligo-catechol Ethylene Glycol Dendrons on Titanium Oxide Surfaces: Adsorption Kinetics, Surface Characterization, and Nonfouling Properties

Torben Gillich,[†] Edmondo M. Benetti,[†,§] Ekaterina Rakhmatullina,[†,∥] Rupert Konradi,[†,⊥] Wen Li,[‡,#] Afang Zhang,[‡,#] A. Dieter Schlüter,[‡] and Marcus Textor*[,†]

[†]Laboratory for Surface Science and Technology, and [‡]Institute of Polymers, Department of Materials, ETH Zurich, Wolfgang-Pauli-Strasse 10, 8093 Zurich, Switzerland

Supporting Information

ABSTRACT: This work covers the synthesis of second-generation, ethylene glycol dendrons covalently linked to a surface anchor that contains two, three, or four catechol groups, the molecular assembly in aqueous buffer on titanium oxide surfaces, and the evaluation of the resistance of the monomolecular adlayers against nonspecific protein adsorption in contact with full blood serum. The results were compared to those of a linear poly(ethylene glycol) (PEG) analogue with the same molecular weight. The adsorption kinetics as well as resulting surface coverages were monitored by ex situ spectroscopic ellipsometry (VASE), in situ optical waveguide lightmode spectroscopy (OWLS), and quartz crystal microbalance with dissipation (QCM-D) investigations. The expected compositions of the macromolecular films were verified by X-ray photoelectron spectroscopy (XPS). The results of the adsorption study, performed in a high ionic strength ("cloud-point") buffer at room temperature, demonstrate that the adsorption kinetics increase with increasing number of catechol binding moieties and exceed the values found for the linear PEG analogue. This is attributed to the comparatively smaller and more confined molecular volume of the dendritic macromolecules in solution, the improved presentation of the catechol anchor, and/or their much lower cloud-point in the chosen buffer (close to room temperature). Interestingly, in terms of mechanistic aspects of "nonfouling" surface properties, the dendron films were found to be much stiffer and considerably less hydrated in comparison to the linear PEG brush surface, closer in their physicochemical properties to oligo(ethylene glycol) alkanethiol self-assembled monolayers than to conventional brush surfaces. Despite these differences, both types of polymer architectures at saturation coverage proved to be highly resistant toward protein adsorption. Although associated with higher synthesis costs, dendritic macromolecules are considered to be an attractive alternative to linear polymers for surface (bio)functionalization in view of their spontaneous formation of ultrathin, confluent, and nonfouling monolayers at room temperature and their outstanding ability to present functional ligands (coupled to the termini of the dendritic structure) at high surface densities.

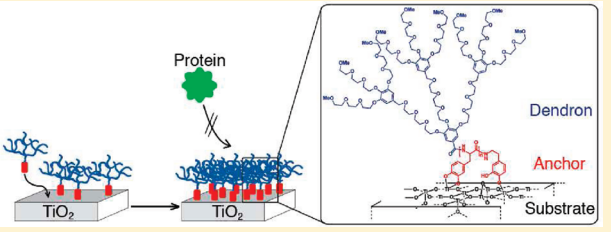

INTRODUCTION

Surface modifications via thin polymer coatings represent an important tool to provide and protect functionality, durability, and reliability of a wide range of materials used for applications such as corrosion and wear protection, medical implants, drug delivery systems, and biosensors. Specifically for the design of biomaterials and biomedical devices, biocompatibility and resistance of surfaces to undesirable nonspecific protein adsorption ("nonfouling" surfaces) are two important requirements that can be achieved by dedicated, usually polymeric surface modification. Synthetic polymers such as poly(ethylene glycol) (PEG),[1] poly(2-methyl-2-oxazoline) (PMOXA),[2] polysaccharides,[3,4] peptidomimetic,[5] and zwitterionic polymers[6,7] with controlled interfacial architecture (high chain surface density, "brush regime") can confer excellent biocompatible and biopassive properties to surfaces. Among them, PEG is the most frequently used polymer for the production of nonfouling surfaces.

The preparation of nonfouling surfaces generally follows one of two approaches, "grafting-from" and "grafting-to" techniques.[8] "Grafting-from" is preferentially used when high polymer densities and/or high layer thicknesses are aimed. This method, however, often requires inert substrates, highly controlled experimental conditions, specialized synthesis knowledge, and cannot always be applied to large substrates. In contrast, the "grafting-to" method is a simple and cost-effective dip-and-rinse procedure, compatible with complex 3D substrate shapes. Additionally, "grafting-to" techniques allow for a precise tailoring of the architecture of adsorbed polymeric films. Molecular weight distributions, branching, and functionalities can be precisely tuned during the synthesis of the molecules assuring the formation of films with well-defined interfacial properties and functions. The polymeric adsorbates require a surface-anchorage

Received: April 9, 2011
Published: June 02, 2011

function in their molecular structure, such as a specific ligand or a surface-active segment, to provide stable attachment of the polymer to the substrate.

On the basis of the grafting-to method, the preparation of PEG-based films has been reported on a variety of organic and inorganic substrates, for example, oligo(ethylene glycol) (OEG)-functionalized alkanethiol self-assembled monolayers (SAMs) on noble metal surfaces such as gold and silver[9−12] and (alkane)phosphate SAMs functionalized with OEG or PEG.[13,14] Furthermore, PEG-catechols have been successfully applied to produce nonfouling TiO_2 and other metal oxide substrates.[15−18]

Catechols, originally inspired by mussel-adhesive proteins[19,20] and bacterial siderophores,[21,22] have found applications as strong anchors for the modification of metal and metal oxide surfaces.[23−25] In other reports, PEG-bearing block-copolymers and graft-copolymers containing surface-active blocks and grafts have also been employed for the deposition of PEG coatings on polymeric materials and metallic surfaces.[26−29]

The biopassive character of PEG-modified surfaces strongly depends on the film thickness, grafting density, and molecular conformation of the grafted polymer chains at the interface. For densely packed OEG-based SAMs, as an example, the mechanism of biopassivity has been reported to directly relate to the coordination of water molecules at the polymer−solvent interface that is controlled by enthalpic factors.[12,30] The partial displacement of these structured water layers by adsorbed proteins is energetically unfavorable. On the other hand, the resistance against protein adsorption of grafted high-molecular weight linear PEG has been proposed to rely on entropy-controlled processes with extensive hydration of long and flexible PEG chains rendering interactions of proteins with the surface unfavorable.[31,32]

In addition to linear polymer grafts, other molecular architectures of PEG such as hyperbranched or star-shaped PEG have recently been reported as alternatives to linear analogues for the preparation of nonfouling surfaces.[33,34] Among the branched macromolecules reported for the modification of surfaces and interfaces, dendrons and dendrimers represent a particularly attractive class of macromolecules due to their regular branching and unique monodisperse structure. Given the interesting ability to incorporate molecules such as drugs or nanoparticles, dendrimers are very attractive as nanocarriers with applications in areas such as contrast agents in magnetic resonance imaging (MRI)[35,36] and computer tomography (CT)[37,38] as well as drug[39−41] and gene delivery systems.[42,43]

Recently, dendritic molecules have attracted increased interest in the context of surface modification for biomedical applications. For example, poly(amido amine) (PAMAM) dendrimers have been chemically bound to SAMs on gold substrates.[44] Such PAMAM adlayers served as protein recognition platforms characterized by enhanced sensitivity if compared to linear SAM analogues. Despite the high potential as surface modifiers, dendritic molecules have, however, rarely been applied for the preparation of nonfouling surfaces. Benhabbour et al. reported that dendronized PEG surfaces resulted in a decrease of protein adsorption if compared to the bare control surface; the reported reduction was, however, rather unsatisfactory.[45] Haag et al. reported on the synthesis of glycerol-based dendrons of generations 1−3 bearing a thiol anchor group for SAM formation on gold surfaces, resulting in favorable biopassive properties.[46]

Despite these first pioneering reports, no quantitative study on the adsorption of dendritic adsorbates with ethylene glycol as building blocks and investigation of the nonfouling properties has been published to the best of our knowledge.

In this work, we report on the synthesis of a novel type of dendritic adsorbates for the modification of metal oxide surfaces based on second-generation OEG dendrons covalently linked to two, three, or four catechols as surface anchors. The synthesized adsorbates were subsequently used to form protein-resistant adlayers on titanium oxide substrates; TiO_2 was chosen as substrate given its relevance for titanium-based medical devices and high-refractive-index optical sensors. The assembly of oligo-catechol OEG dendrons on the metal oxide interface was monitored by ex situ variable angle spectroscopic ellipsometry (VASE), in situ quartz crystal microbalance with dissipation (QCM-D), and optical waveguide lightmode spectroscopy (OWLS). The chemical composition of the dendron-modified substrates was characterized by X-ray photoelectron spectroscopy (XPS). Surface coverage, hydration, and stability of the prepared adlayers were studied quantitatively as a function of the number of catechol units in the anchor moiety and were compared to a linear PEG analogue of comparable molecular weight.

Furthermore, full blood serum was used to test the resistance against unspecific protein adsorption of the titanium oxide surfaces modified with the dendritic and linear adsorbates. The results were correlated with the surface coverage and the interfacial macromolecular architecture. This study reveals how the molecular structure of the adsorbates influences the adsorption kinetics, degree of film hydration, viscoelasticity of the adlayer, protein resistance, and surface stability in physiological buffer solution. Despite lower film thickness, reduced hydration, and increased stiffness when compared to the linear PEG analogues, excellent nonfouling properties of the OEG dendronized surfaces are obtained when the anchor is composed of multiple catechol units.

MATERIALS AND METHODS

Materials. 2-Propanol (LiChrosolv, gradient grade for HPLC) was purchased from Merck. Toluene (HPLC grade) was obtained from Acros Chemicals. Cleaner solution (300 mmol/L HCl, 1% detergent, Cobas Integra) was purchased from Roche Diagnostics. Nitrogen (≥99.999%) was obtained from PanGas (Dagmarsellen, Switzerland). 4-(2-hydroxyethyl) piperazine-1-ethanesulfonic acid (HEPES) and 3-(*N*-morpholino)propanesulfonic acid (MOPS) were obtained from Fluka Chemika. All water used for surface experiments and buffer solutions was prepared by a Millipore water purification system (Milli-Q system; Millipore, 18.2 Ω, TOC ≤ 5 ppb). Full blood serum solution (Precinorm U, Cobas, Roche Diagnostics) was prepared freshly with Millipore water and filtered prior use. The second-generation OEG-based dendrons with carboxylic acid (G2-COOH) and pentafluorophenol active ester (G2-PFP) at the focal point were synthesized according to previously reported procedures.[47,48] Cyclohexene and tetrahydrofuran (THF) were distilled prior use. PEG-2300 Da-NHS (methoxy poly(ethylene glycol) carboxy methyl ester, MW 2300 Da) was purchased from JenKem Technology (U.S.). Other reagents and solvents were purchased at reagent grade and used without further purification. Silica gel 60 (230−400 mesh, Fluka Chemika) was used as stationary phase for column chromatography. Thin layer chromatography plates (silica gel 60 with fluorescent indicator UV_{254} coated on aluminum sheets 0.20 mm) were purchased from Macherey-Nagel (Düren, Germany).

Chemical and Physical Characterization. Preparative gel-permeation chromatography (GPC) (Japan Analytical Industry Co. Ltd., LC 9101, Hitachi pump L-7110, flow rate of 3.5 mL/min, RI detector Jai RI-7, UV-detector Jai UV-3702, 280 nm, two columns Jaigel

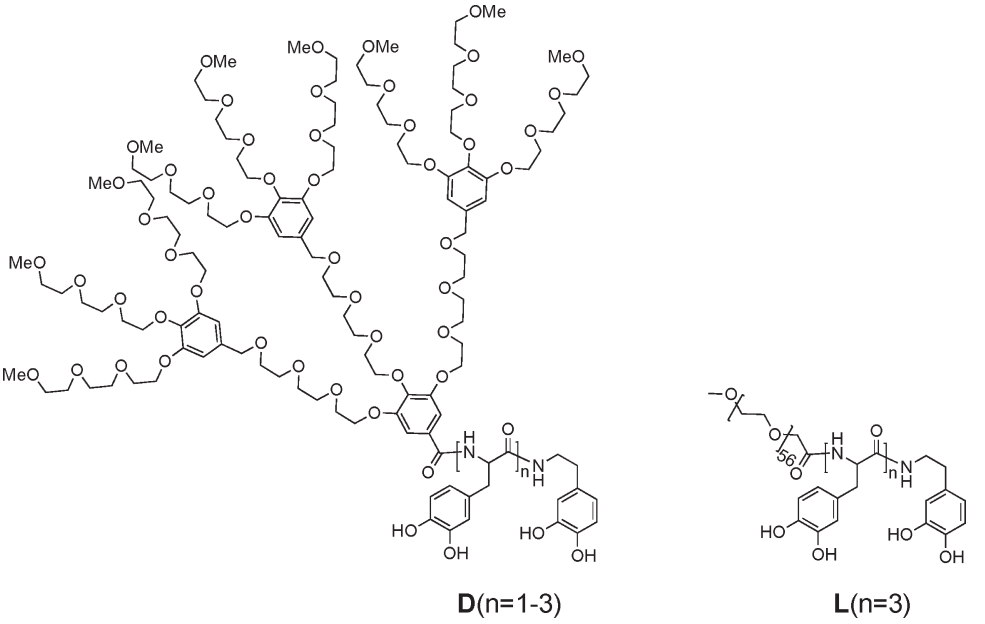

Figure 1. Chemical structure of the second-generation (G2) ethylene glycol dendrons covalently coupled to surface-active oligo-catechol anchors, **D**(n = 1−3), and the linear (control) PEG polymer, **L**(n = 3), of similar molecular weight (polymerization degree of 56).

2H and 2.5H, 20 × 600 mm for each, $CHCl_3$ at room temperature) was used for purification of the final compounds **D**(n = 1−3) and **L**(n = 3) (molecular structures are shown in Figure 1). **D**(n = 1−3) symbolizes the G2 OEG-based dendron types that carry a dimeric (n = 1) to tetrameric (n = 3) oligo-catechol unit at the focal point. **L**(n = 3) represents a linear PEG chain, which at one terminus carries a tetrameric catechol unit. ^{1}H and ^{13}C NMR spectroscopic measurements were recorded on Bruker Avance 300, 500, and 700 spectrometers (^{13}C NMR frequencies of 75.5, 126, or 176 Hz, respectively) at room temperature. The signal from the specific solvent was used as an internal standard for the determination of the chemical shift (chloroform-d, ^{1}H 7.26 ppm, ^{13}C 77.36 ppm; dichloromethane-d_2, ^{1}H 5.33 ppm, ^{13}C 54.24 ppm; dimethylsulfoxide-d_6, ^{1}H 2.54 ppm, ^{13}C 40.45 ppm; deuteriumoxide-d_2, ^{1}H 4.79 ppm; acetonitrile-d_3, ^{1}H 1.96 ppm, ^{13}C 1.79 ppm; methanol-d_4, ^{1}H 3.34 ppm, ^{13}C 49.86 ppm). Mass spectrometry measurements were performed by the MS-service of the Laboratory for Organic Chemistry at ETH Zürich (MALDI-TOF, Bruker UltraFlex II; MALDI-FTICR-MS, IonSpec (Varian) Ultima; HiResESI, Bruker Daltonics maxis, UHR-TOF). Elemental analysis measurements were performed by the Micro-Laboratory of the Laboratory for Organic Chemistry at ETH Zurich. UV−vis measurements for cloud-point determination were performed on a Cary 1E spectrometer (Varian, U.S.). The cloud-point was determined at a dendron/polymer concentration of 0.1 mg/mL in cloud-point buffers CP and/or CP* (CP = 0.1 mol/L MOPS, 0.5 mol/L NaCl, 0.5 mol/L K_2SO_4, H_2O, pH = 6; CP* = 0.1 mol/L MOPS, 0.5 mol/L K_2SO_4, H_2O, pH = 6) with a heating rate of 0.2 °C/min at a wavelength of 500 nm. The cloud-point temperature (T_C) is defined as the temperature where the absorbance of 0.001 relative to the baseline is reached (sharp increase of the absorbance, see Figure S1). The T_C values of the different compounds (average of two independent measurements) are compiled in Table 1.

Sample Preparation. Silicon wafer slides were purchased from Si-Mat (Landsberg, Germany) and cut in 10 × 10 mm^2 squares before use. Gold-coated QCM-D crystals were purchased from Q-Sense (Sweden). Commercial grating-coupler OWLS waveguide chips (with SiO_2/TiO_2 waveguiding layer) were purchased from MicroVacuum (Budapest, Hungary). All substrates including the QCM-D and OWLS sensor chips were coated with a thin TiO_2 layer deposited by reactive magnetron sputtering (PSI Villigen, Switzerland). The thickness of TiO_2 layer was around 20 nm for the silicon wafer and 6 nm for the QCM-D crystals and the OWLS waveguides. Prior to surface modification, the substrates were sonicated for 10 min in toluene, twice in 2-propanol, and finally dried under a stream of nitrogen. Subsequently, they were treated for 40 min in a preheated UV-ozone cleaner (UV-clean, Boekel Instruments, U.S.). Substrates for ellipsometry measurements were only used once. QCM-D crystals and OWLS waveguides were reused several times; following every QCM-D and OWLS measurement, the sensor crystals and OWLS waveguides were sonicated in cleaner solution (300 mmol/L HCl, 1% detergent, COBAS INTEGRA, Roche Diagnostics) for 10 min and later incubated for 50 min without sonication. Finally, the sensors were immersed in 0.1 mol/L aqueous HCl solution for 3 h, rinsed with Milli-Q water, and dried under a stream of nitrogen.

Table 1. Molecular Weights and Cloud-Point Temperatures (T_C) of the Different Macromolecules Measured in the Specific Buffer (CP and CP*) at a Heating Rate of 0.2 °C/min[a]

compound code	molecular weight (M_W)	buffer	T_C (°C)
D(n = 1)	2610.95 g/mol	CP	46.2 ± 0.9
D(n = 2)	2790.12 g/mol	CP	28.0 ± 0.2
D(n = 3)	2969.29 g/mol	CP*	27.9 ± 0.2
		CP	19.2 ± 0.2
L(n = 3)	3229.79 g/mol (x = 56)	CP	62.0 ± 2.8

[a] For **L**(n = 3), x = 56 (x = repeating unit of the most intense peak in the MALDI-TOF spectra) was used to calculate the molecular weight of the compound.

Ellipsometry. In this study, ex situ ellipsometry measurements were carried out with a variable angle spectroscopic ellipsometer (M-2000F, Woollam Co., Inc., Lincoln, NE). The measurements were performed in the spectral range of 370−1000 nm at three different angles of incidence (65°, 70°, and 75°). Each data point resulted from the average of at least 50 measurements, and the obtained sensorgrams were fitted with a four-layer model (Si, SiO_2, TiO_2, and organic adlayer) using the analysis software WVASE32. The thickness of Si and SiO_2 layers was assumed to be constant. The TiO_2 layer was fitted before adsorption using the

oscillator model; the organic adlayer was fitted using the Cauchy model (A_n = 1.45, B_n = 0.01, and C_n = 0).[49] The reported layer thickness is the average over at least three different samples. The obtained layer thickness was converted into dry mass values by applying the following formula (I): $m = d \times l \times A^2$, m = adsorbed mass [ng], d = adlayer density [ng], l = layer thickness [cm], A^2 = area unit [cm^2]. A homogeneous mass distribution of the organic adlayer perpendicular to the TiO_2 surface was assumed with a density of 1.08 g/cm^3 for the dendron and PEG adlayer.[49]

In a standard ellipsometry adsorption experiment, the freshly cleaned samples were incubated in a plastic well plate (diameter of the well: 1.5 cm, TPP, Trasadingen, Switzerland) with 0.5 mL of sample solution (0.1 mg/mL) in cloud-point buffer (for **D**(n = 1), **D**(n = 2), and **L**(n = 3) in CP; for **D**(n = 3) in CP*) at room temperature (22−23 °C). After the specific adsorption time, 1 mL of HEPES 2 buffer (0.1 mol/L HEPES, pH = 7.4, 150 mmol/L NaCl, H_2O) was added, and each sample was transferred into another well containing 1 mL of HEPES 2 buffer and incubated for 40 min. Subsequently, the sample was rinsed with Milli-Q water, dried under a stream of nitrogen, and the layer thickness was measured with ellipsometry. All solutions used for surface modification were filtered through a 0.2 μm syringe filter (cellulose acetate, Minisart, Sartorius Stedim). Because the cloud-point temperature of **D**(n = 3) was 19.2 °C in CP buffer and therefore lower than the adsorption temperature of 22−23 °C, the adsorption buffer CP* with lower ionic strength was used for the adsorption of **D**(n = 3) to increase the cloud-point temperature to 27.9 °C.

OWLS. OWLS (OWLS110, MicroVacuum Ltd., Budapest, Hungary) is a label-free biosensor technique that allows the in situ investigation of molecular adsorption. Measurement principles and quantification of the adsorbed mass have been described in the literature.[50] The refractive index increment, dn/dc, was determined for each macromolecule using a differential refractometer (Atago RX-5000α) in the appropriate buffer. This molecule- and buffer-specific dn/dc value was used to determine the change of the effective refractive units (ΔRU) of the particular molecule. A detailed description for the determination of the dn/dc values is given in the Supporting Information (Table S1).

The adsorption experiments were performed at 25 °C. In a standard experiment, the cleaned waveguide chips were inserted in the flow cell and immediately incubated in HEPES 2 buffer. After baseline equilibration overnight, cloud-point buffer (CP or CP*) was pumped into the flow-cell. After the second-baseline equilibration, the adsorbate solution was pumped into the flow-cell (∼0.60 mL/min, 0.8 mL) and the adsorption was run under continuous flow conditions (∼0.12 mL/min). After adsorption, the polymer solution was replaced by cloud-point buffer (∼0.60 mL/min, 2 mL) followed by HEPES 2 buffer. For the subsequent testing of the protein resistance of the polymer-modified surface, the flow-cell was filled with full blood serum and incubated for 20 min before rinsing with HEPES 2 buffer.

QCM-D. Quartz crystal microbalance with dissipation (QCM-D) measurements were carried out on a Q-Sense E4 (Q-Sense, Sweden) equipped with a multichannel pump (IPC Ismatec SA, Switzerland). This surface-sensitive technique is used to monitor adsorption kinetics through changes in resonance frequency and energy dissipation on an oscillating piezoelectric quartz crystal sensor. Changes of the resonance frequency (Δf) of the crystal reflect adsorbed mass, while energy dissipation (ΔD) provides information on the viscoelastic properties of the adsorbed layer. In contrast to optical techniques such as ellipsometry and OWLS, the change of the resonance frequency Δf in QCM-D measurements includes solvent molecules (here water) that are mechanically coupled to the surface. Combining the results of ellipsometry and QCM-D allows one to estimate the degree of solvation (hydration) of the adsorbed adlayer.

In a standard adsorption experiment, the cleaned crystals were immediately inserted into the flow chambers (volume of flow chamber: 79 μL) and incubated with HEPES 2 buffer. After baseline equilibration in HEPES 2 buffer (∼2−3 h), cloud-point buffer was pumped into the flow chambers, and a second baseline was recorded before the adsorbate solution (0.1 mg/mL of **D**(n = 1−3) or **L**(n = 3) in cloud-point buffer) was pumped into the flow chambers (∼0.6 mL/min, 0.8 mL). After a specific adsorption time, the flow chambers were rinsed with cloud-point buffer followed by HEPES 2 buffer (∼0.6 mL/min, 2 mL). The frequency change of the HEPES 2 buffer baseline and the value obtained after rinsing with HEPES 2 buffer were used to determine the hydrated mass of the adsorbed adlayer. The complete sensorgram of an exemplary QCM-D experiment is shown in the Supporting Information, Figure S4. All experiments were performed at 25 °C in a stop-flow mode, and the third, fifth, seventh, ninth, 11th, and 13th overtones were recorded. For calculating the adsorbed mass (Δm) of the hydrated dendritic adlayer (**D**(n = 1−3), the Sauerbrey model was used ($\Delta m = C \times \Delta f$, where Δm = adsorbed mass [ng/cm^2], C = −17.7 ng/(cm^2 × Hz) = sensitivity constant of the quartz crystal, Δf = overtone-normalized frequency change). For reproducibility reason, only the fifth overtone, normalized to the fundamental resonance, was used to calculate the adsorbed mass and to determine the dissipation changes ΔD. For the case of linear **L**(n = 3), the Voigt model for viscoelastic adlayers was used to calculate the adsorbed mass with help of the software QTools 3. For the determination of the hydrated layer thickness, the viscosity of the surrounding fluid (0.998 kg/m × s) and the density of the hydrated adlayer (1.020 g/cm^3) were handled as fixed parameters during the fitting procedure.

XPS. X-ray photoelectron spectroscopy (XPS) was performed on a Sigma2 Probe Thermo XPS (Thermo Scientific, UK) with a nonmonochromatic AlK_α source operated at 300 W. The instrument was equipped with a hemispherical analyzer and a multichannel detector. The sample was illuminated by the source at an angle of 54°, while the electron takeoff angle is 0° relative to the surface normal. For each sample, a survey spectrum (1 eV scan/step, 2 scans) and high-resolution spectra (0.1 eV/step; C [9 scans], N [49 scans], O [9 scans], Si [2 scans], Ti [3 scans]) were recorded at an analyzer pass energy of 25 eV and a dwell time of 50 ms. All spectra were calibrated by setting the signal of the aliphatic C signal at 284.7 eV (rather than 285.0 given the high proportion of aromatic carbon in the compounds). Curve fitting was carried out using CasaXPS software [version 2.3.15, www.casaxps.com] with Gaussian−Lorentzian functions and Shirley background subtraction, assuming a homogeneous surface composition. Published atomic sensitivity factors[51] were used to convert the measured intensities to normalized intensities and to quantify the atomic surface composition of the analyzed samples. Samples used for XPS analysis were incubated for 48 h in the corresponding adsorbate solution, and afterward equilibrated in 0.5 mL of HEPES 2 solution for 40 min and rinsed with water. The quantitative values provided are averages based on the measurements of two different, independent samples.

Stability Test. The stability of dendron and linear PEG films in physiological solutions was monitored by ellipsometry. The samples were incubated in the adsorbate solution (0.1 mg/mL in cloud-point buffer) for 24 h. The modified substrates were subsequently incubated in 0.5 mL of HEPES 2 solution for 40 min. Subsequently, the samples were rinsed with Milli-Q water, dried under a stream of nitrogen, and the initial layer thickness was measured by ellipsometry. Each sample was further incubated in 3 mL of HEPES 2 buffer solution, and the layer thickness was measured after 72, 96, and 288 h. The remaining thickness value measured for each layer resulted from the average obtained for three independent samples.

Resistance to Serum Adsorption. Functionalized substrates were first immersed in 1 mL of HEPES 2 solution for 15 min and subsequently incubated in 250 μL of full blood serum. After 20 min incubation time, 1 mL of HEPES 2 buffer was added, and each sample was transferred in a clean well containing 1 mL of HEPES 2 solution and left incubating for 20 min. The samples were finally rinsed with Milli-Q water, dried under a stream of nitrogen, and analyzed by ellipsometry.

Scheme 1. Synthesis of the Oligo-catechol-Based Anchor Groups 6c, 7c, and 8c[a]

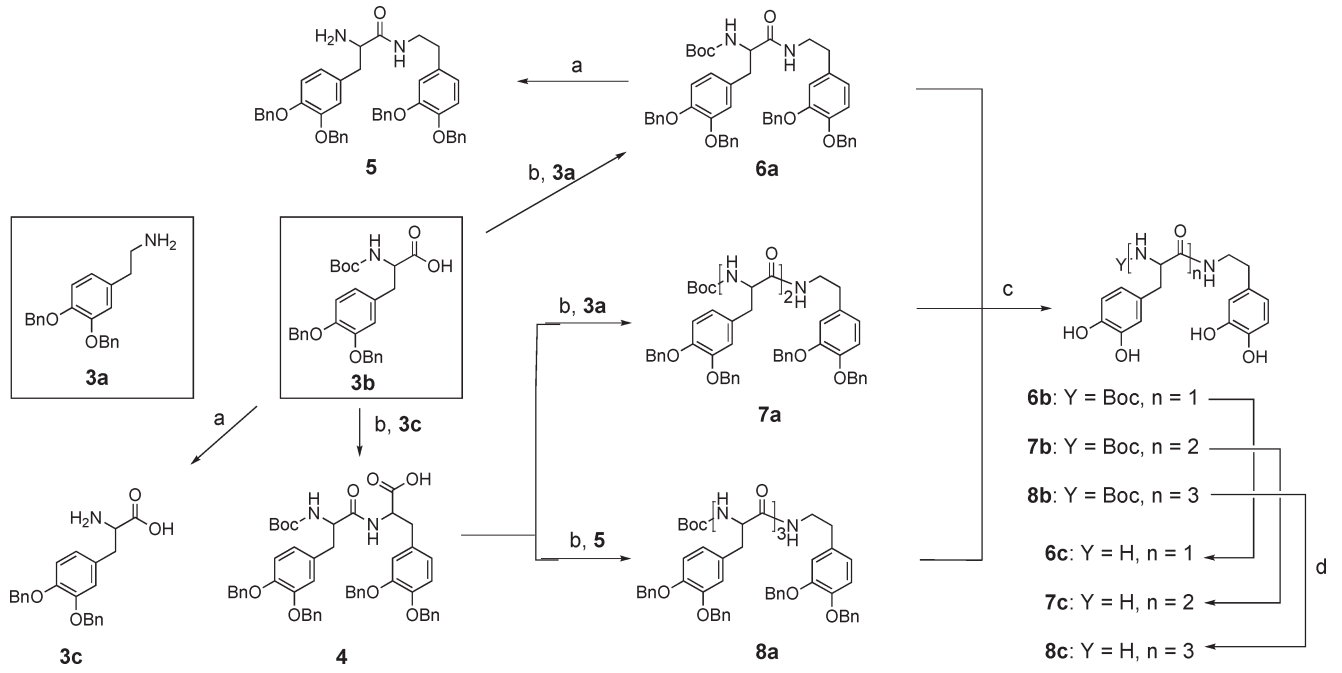

[a] Molecules **3a** and **3b** were synthesised according to refs 52 and 53, respectively. Reagents and conditions: (a) 4 N HCl in dioxane, 0 °C, 2 h, (99%); (b) EDC, NHS, *N*-methylmorpholine, CH_2Cl_2, 0 °C to room temperature, overnight (57% [**4**], 66% [**6a**], 64% [**7a**], and 61% [**8a**]); (c) cyclohexene, 10% Pd/C, EtOH/THF, 85 °C, 2.5 h (76% [**6b**], 50% [**7b**], and 74% [**8b**]); (d) 1.25 N HCl in MeOH, 0 °C, 3 h (98%).

Each data point is the average from the measurements of at least three different samples.

RESULTS AND DISCUSSION

Synthesis of Adsorbates. Ethylene glycol dendrons with oligo-catechol binding units were synthesized to obtain strongly binding adsorbates for the modification of titanium oxide substrates. The anchor groups are based on catechol oligomers, specifically L-3,4-dihydroxyphenylalanin (L-DOPA) and 3-hydroxytyramine (Dopamine), which are known to strongly interact with titanium oxide surfaces. Dendritic molecules with triethylene glycol building blocks and two (**D**(n = 1)), three (**D**(n = 2)), and four (**D**(n = 3)) catechol units in the binding moiety were synthesized (Figure 1). In addition, the synthesis of a linear PEG analogue (**L**(n = 3), M_w = 3229.79 g/mol) with a molecular weight comparable to the one of the dendritic macromolecule **D**(n = 3) (M_w = 2969.29 g/mol) was performed, allowing us to compare the surface properties of the two different PEG/OEG-based molecular architectures.

The synthesis path to the three different catechol oligomers **6c**, **7c**, and **8c** is shown in Scheme 1. It was based on the use of orthogonal protecting group strategy and standard amide-bond formation. The detailed synthetic descriptions for all molecules are presented in the Supporting Information. The purity of the synthesized molecules was confirmed by ^{1}H and ^{13}C NMR spectroscopy, mass spectrometry, and elemental analysis measurements. It is noteworthy that similar catechol-based oligomers have already been reported.[15] They differ from the ones presented here in that the former carry a carboxylic acid function at the terminal catechol unit and moreover use protecting groups that are not strictly orthogonal. Our approach has two main advantages. First, no free carboxylic acid functions were included in the molecular structure of the adsorbates to account for the potentially detrimental impact on the adsorption behavior.[18] Second, our synthetic strategy proceeded by exclusively using orthogonal protecting groups, which in principle opens the opportunity to synthesize even longer oligomers, if required.

Scheme 2 depicts the conversion of these catechol-based oligomers to the *N*-dendronized target compounds **D**(n = 1−3) shown in Figure 1, as well as the synthesis of the linear PEG-based analogue **L**(n = 3) presenting the same anchoring unit as for **D**(n = 3).

The synthesized dendron/PEG-catechol conjugates were purified by preparative GPC to remove surface-active uncoupled anchor groups (**6c**, **7c**, and **8c**) and high molecular weight side-products. These side-products are most likely the result of the oxidation and the subsequent uncontrolled cross-linking reaction of the catechol moieties.[18,54,55] The exemplary GPC elugram of the **D**(n = 3) purification is shown in the Supporting Information, Figure S9. There, it was possible to separate the starting material G2-PFP and its partially hydrolyzed analogue, G2-COOH, from the surface active compound **D**(n = 3). In case of **D**(n = 2), only a partial separation could be achieved. For the molecules **D**(n = 1) and **L**(n = 3), purification from the uncoupled starting compound or the hydrolyzed activated ester was not possible. Nevertheless, adsorption tests based on in situ optical waveguide lightmode spectroscopy (OWLS) proved that molecules G2-COOH, PEG-2300 Da-NHS, and PEG-2300 Da-COOH were not surface-active and did not influence the adsorption experiments (see Supporting Information, Figure S3). The final products were analyzed by ^{1}H and ^{13}C NMR spectroscopy, mass spectrometry, and elemental analysis measurements. The absence of the surface-active free amines **6c**, **7c**, and **8c** was tested and proved by thin layer chromatography. The amount of the **D**(n = 1−3) and **L**(n = 3) in the product mixture was

dx.doi.org/10.1021/ja202760x |*J. Am. Chem. Soc.* 2011, 133, 10940–10950

Scheme 2. Synthesis of the Final Compounds D(n = 1−3) and L(n = 3)[a]

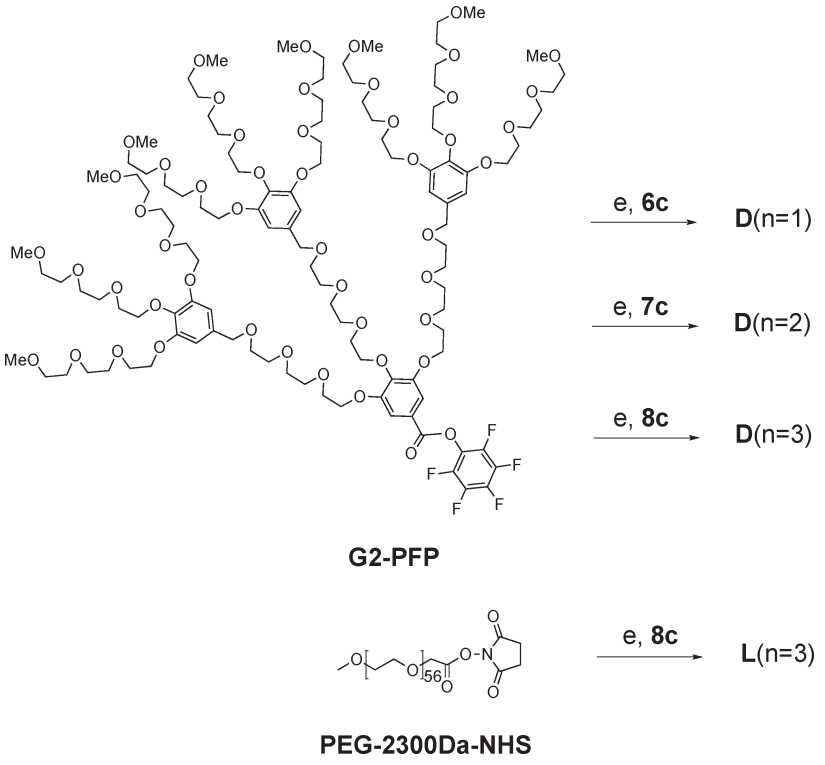

[a] Reagents and conditions: (e) NEt_3, DMF, 0 °C to room temperature, 6−10 h (8% D(n = 3), 17% D(n = 2), 51% D(n = 1), and 22% L(n = 3)).

calculated by ^{1}H NMR spectroscopy. The concentration of the surface-active compounds D(n = 1−3) and L(n = 3) in the purified product mixture was calculated as 99, 92, 79, and 75 mol % for D(n = 3), D(n = 2), D(n = 1), and L(n = 3), respectively (see the Supporting Information for quantification procedure, Figure S10). The compounds **6a**, **7a**, and **8a** were prepared at the few gram scale and the final products D(n = 1−3) and L(n = 3) on the 15−70 mg scale.

Adsorption Kinetics and Surface Coverage (Ellipsometry, OWLS). The adsorption of the dendritic D(n = 1−3) and linear L(n = 3) compounds on TiO_2 surfaces was monitored by ellipsometry and OWLS. While the ex situ ellipsometry data are particularly useful in providing information on the kinetics over longer time periods (Figure 2, up to 72 h), OWLS data allow the in situ analysis of the initial adsorption kinetics (Figure 3, up to 60 min). The dry layer thickness values measured by ellipsometry were also converted to dry adsorbed mass assuming a given density for the organic adlayer and the formation of a homogeneous film (see Materials and Methods for details). These data are compiled in Table 2. The formation of a homogeneous adlayer was confirmed by atomic force microscopy (AFM) (see Supporting Information, Figure S6).

Dendritic Adsorbates. The ellipsometry film-thickness versus time curves (Figure 2 and Table 2) demonstrate that the molecular adsorption process followed a two-step regime. Within the first 10−30 min of incubation, high adsorption rates were observed for the dendritic D(n = 1−3) adsorbates; after 30 min, 72%, 76%, and 90% of the maximum (72 h) layer thickness (corresponding to 9.6, 13.0, and 17.2 Å) were obtained for D(n = 1), D(n = 2), and D(n = 3), respectively. After this first, fast adsorption stage, thickening rates decreased significantly, and a slow increase of layer thickness was observed over the following

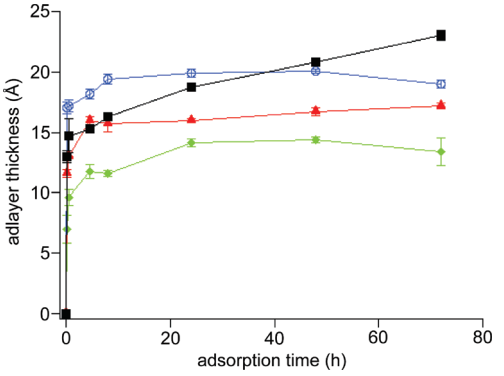

Figure 2. Polymer adlayer thicknesses on TiO_2-coated silicon wafers measured by ellipsometry as a function of adsorption time for compounds D(n = 1), green ◆, D(n = 2), red ▲, D(n = 3), blue ⊙, and L(n = 3), ■. Error bars are often smaller than the symbol size for some measurement points.

hours of incubation, with D(n = 2) and D(n = 3) reaching saturation values earlier in comparison to D(n = 1) (Table 2).

The in situ OWLS adsorption study confirmed in more detail the high adsorption rates within the first 30 min of incubation and demonstrated characteristic differences between the different adsorbates (Figure 3). Interestingly, the initial adsorption rates depended on the number of catechol units in the anchor group of the dendrons, with their slopes increasing significantly with the number of catechols in the anchor group (Figure 3). This was also reflected in the layer thicknesses measured after 30 min by ellipsometry (Table 2).

The adlayer thickness values at saturation also depended on the type of the dendrons, increasing with the number of catechol

groups, from 13.4 Å for **D**(n = 1) to 17.2 Å for **D**(n = 2), to 19.0 Å for **D**(n = 3) (Table 2).

Linear Adsorbates. The adsorption profile of the linear analogue **L**(n = 3) showed clear differences from the ones of the dendrons. The initial adsorption rate was found to be considerably lower if compared to the dendritic compound with the same anchor moiety, **D**(n = 3) (Figure 3). This is in good agreement with the measured layer thickness after 30 min of adsorption, that is, 17.2 Å for **D**(n = 3) and 14.8 Å for **L**(n = 3) corresponding to 90% and 64% of the final thickness values (Table 2). Furthermore, the adlayer thickness of **L**(n = 3) after the first 30 min steadily increased with nearly linear kinetics, not reaching a clear plateau value even after 72 h of adsorption time. The (still increasing) surface adlayer thickness for the compound **L**(n = 3) after 72 h adsorption time was found to be slightly higher (23.0 Å) in comparison to 19.0 Å found for **D**(n = 3).

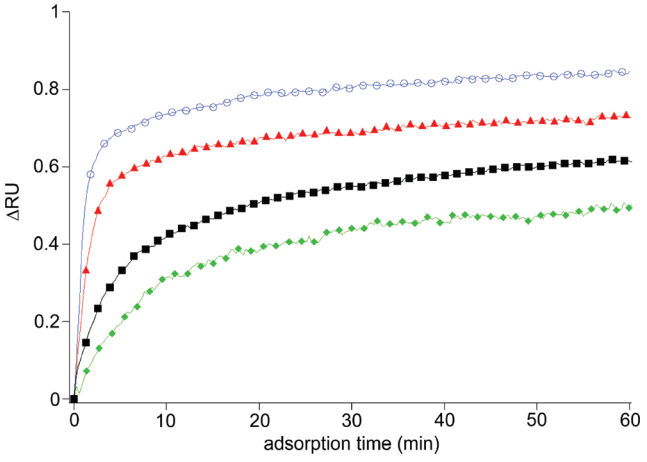

Figure 3. OWLS sensorgrams of the adsorption of **D**(n = 1), green ◆, **D**(n = 2), red ▲, **D**(n = 3), blue ⊙, and **L**(n = 3), ■, in cloud-point buffer. ΔRU = change in effective refractive units. For clarity reasons, only every fifth measurement point is illustrated. Substrate: TiO_2-coated waveguide chips.

Discussion of Dendritic versus Linear Adsorbate Properties. All four compounds were found to assemble with a fast initial (<30 min) and much slower second-stage adsorption rate. The different initial adsorption rates for **D**(n = 1−3) imply that diffusion from the solution to the titania surface is not the rate-limiting step (molecular weights are quite similar), rather that the probability of "irreversible" binding to the substrate ("sticking coefficient") increases with increasing number of catechols in the anchors. This observation can be related to the reversibility of the single catechol−TiO_2 interaction as it has been already experimentally verified[16,56] and the formation of an essentially irreversible multivalent catechol binding, which is likely to strongly increase with increasing number of catechols in the anchor group.[15]

The comparatively slower initial adsorption rate observed for the compound **L**(n = 3) and its subsequent very slow uptake regime extending to beyond 72 h can be understood as reflecting three physical differences between the two classes of macromolecules: (a) The high conformational flexibility of the linear polymer chains reduces the probability that the anchor is well exposed and can bind within the time of residence at the surface, resulting in lower "sticking probability" (even at low coverage) when compared to the conformational much less flexible, stiffer dendritic molecule with improved presentation of the anchor. (b) The relatively large radius of gyration of the linear, highly hydrated PEG polymer is expected to reduce the adsorption kinetics at higher coverage when adsorption to the surface becomes increasingly hampered by steric interaction with already adsorbed polymer molecules, resulting in slow adsorption kinetics. With the smaller, structurally more confined dendrons, organization at the interface should proceed with greater ease. (c) The problem of slow adsorption kinetics at higher surface coverage is a well-known practical limitation that has been partly overcome by grafting polymers to surfaces under so-called cloud-point condition (buffers of high ionic strength and temperatures close to the cloud-point) where polymers with an inverse solubility−temperature relationship lose part of their bound water and collapse, resulting in faster adsorption kinetics at especially high surface coverage.[57] We performed adsorption of

Table 2. Compilation of the Ellipsometry and QCM-D Results for the Different Adsorbates[a]

molecule	adsorption time	layer thickness (Å)	dry mass (ng/cm^2)	molecule density (1/nm^2)	EG density (1/nm^2)	hydrated mass (ng/cm^2)	hydrated layer thickness (Å)	hydration (wt %)
D(n = 1)	30 min	9.6 ± 0.6	104 ± 7	0.24	8.6			
	4.5 h	11.8 ± 0.6	127 ± 6	0.29	10.5	244 ± 22	23.2 ± 2.1	48
	72 h	13.4 ± 1.2	145 ± 13	0.33	12.0			
D(n = 2)	30 min	13.0 ± 0.0	140 ± 0	0.30	10.9			
	4.5 h	16.0 ± 0.4	172 ± 4	0.37	13.4	297 ± 6	28.3 ± 0.6	42
	72 h	17.2 ± 0.3	186 ± 3	0.40	14.5			
D(n = 3)	10 min	17.1 ± 0.5	184 ± 5	0.37	13.4	296 ± 6	28.2 ± 0.1	38
	30 min	17.2 ± 0.5	186 ± 6	0.37	13.6	316 ± 9	30.2 ± 0.1	41
	4.5 h	18.1 ± 0.4	196 ± 5	0.40	14.3	340 ± 15	32.4 ± 1.4	42
	72 h	19.0 ± 0.3	206 ± 3	0.42	15.0			
L(n = 3)	10 min	13.0 ± 0.5	141 ± 6	0.26	14.7	642 ± 9	63.0 ± 0.9	78
	30 min	14.8 ± 1.4	159 ± 15	0.30	16.6	673 ± 17	65.9 ± 1.6	76
	4.5 h	15.3 ± 0.3	165 ± 3	0.31	17.2	751 ± 15	73.7 ± 1.4	78
	72 h	23.0 ± 0.4	249 ± 5	0.46	26.0			

[a] The dry layer thickness was converted to dry mass values by assuming a density of 1.08 g/cm^3 of the dried organic adlayer. The adsorbed hydrated mass was obtained from QCM-D measurements performed under physiological conditions (HEPES 2 buffer: 0.1 mol/L HEPES, pH = 7.4, 150 mmol/L NaCl). The hydration was estimated by subtracting the dry mass from the hydrated mass.

all adsorbates in a cloud-point buffer (CP and CP*) at room temperature. For **L**(n = 3), a compound with a cloud-point of 62 °C, room temperature is insufficient to provide a beneficial clouding effect during the adsorption process, in stark contrast to the dendritic compounds. These have much lower cloud-points, in particular **D**(n = 2) and **D**(n = 3) for which the cloud-points (~28 °C) are expected to be close enough to the adsorption temperature to facilitate the adsorption and the formation of a dense molecular packing at the surface due to the further reduced hydration and size. In a control experiment, molecule **D**(n = 3) was adsorbed at room temperature in a (noncloud-point) standard buffer (HEPES 2), and adsorption kinetics was indeed found to be slower than the ones under cloud-point condition (for details, see Supporting Information, Table S2).

Regarding the saturation surface coverage achieved after sufficiently long adsorption time, there is a clear dependence of the layer thicknesses on the number of catechol groups for the dendrons **D**(n = 1−3), increasing from n = 1 to n = 3. Thermodynamically, there is a balance between the effective adhesion energy and the steric-repulsive penalty, which increases with increasing molecular surface density. The increasing surface coverage with increasing n is therefore believed to reflect this balance demonstrating the importance of catechol multivalency for strong surface affinity. A very similar observation has been reported for the poly(L-lysine)-*graft*-poly(ethylene glycol) (PLL-*g*-PEG) system and theoretically verified in a molecular modeling study by self-consistent field theory.[58]

Assembly of both **D**(n = 3) and **L**(n = 3) resulted in very low protein adsorption (see below), implying a dense brush regime and low defect density. This is generally believed to require surface mobility of adsorbates. Models such as the random sequential adsorption (RSA) model,[59] not considering surface mobility, result in a surface coverage well below full coverage, which would lead to substantial protein adsorption. Surface mobility of catechol-based anchors has not been investigated in this work, but considered to be plausible on the basis of the observed reversibility of the single catechol−titanium ion bond and the theoretically predicted dynamics associated with a switch between bidentate and monodentate coordination regimes.[60,61]

Layer Hydration (QCM-D). The QCM-D technique is a useful tool in providing information on the (hydrated) adsorbed mass and the viscoelastic properties of surface adlayers. While the ellipsometry measurements provide information about the dry thicknesses and therefore the adsorbed dry masses, QCM-D frequency changes include contributions from water molecules that are mechanically coupled to the surface adlayer. Therefore, the difference between QCM hydrated mass (calculated with Sauerbrey or Voigt model) and ellipsometry dry mass has been successfully used as a quantitative measure of the film hydration.[62] Independent measurements of the hydration of PLL-*g*-PEG brush layers using the surface force apparatus (SFA)[63] and colloidal-probe AFM spectroscopy[64] have shown excellent agreement with the approach used in this study.

Figure 4 (lower part) shows the frequency shift Δf for the adsorption of the three dendritic adsorbates **D**(n = 1−3) and the linear polymer **L**(n = 3) as a function of adsorption time up to 4.5 h. For the dendritic adsorbates **D**(n = 1−3), the adsorbed mass (Δf change), at a given time point, increases with the number of catechols in the anchor part in agreement with the experimental findings derived from ellipsometry and OWLS measurements (compare Figure 4 with Figures 2 and 3). Different from the results of the latter investigations, however, the QCM-D frequency

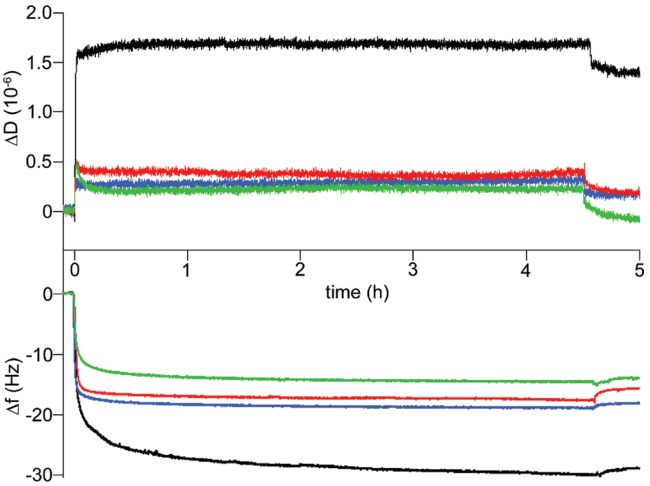

Figure 4. QCM-D sensorgrams of the adsorption of **D**(n = 1) (green), **D**(n = 2) (red), **D**(n = 3) (blue), and **L**(n = 3) (black) on TiO_2-coated QCM-D crystals, 4.5 h adsorption time. Frequency shift (Δf, lower part of the figure) and dissipation change (ΔD, upper part) are shown as a function of adsorption time. Adsorption experiments were carried out at 25 °C in cloud-point buffer. After 4.5 h adsorption time, the flow cell was subsequently rinsed with cloud-point buffer followed by HEPES 2 buffer (not shown in this figure; complete sensorgram is shown in Figure S4) to remove weakly physisorbed adsorbates.

change for the **L**(n = 3) polymer is approximately 60% higher in comparison to **D**(n = 3).

Dry thickness, dry mass, wet mass, and hydration values (the latter as the difference between wet and dry mass, see Materials and Methods section) for all adsorbates and adsorption times up to 4.5 h are compiled in Table 2. Interestingly, surface-grafted dendritic molecules showed a degree of hydration of around 40 wt %, approximately independent from adsorption time or surface coverage. This is in contrast to the twice as high hydration level of ca. 80 wt % for polymer **L**(n = 3), a value that has also been found to be typical for other (linear) PEG-brush surfaces.[62,63,65]

Figure 4 (upper part) displays the measured ΔD values as a function of incubation time for the different adsorbates. The adsorbed dendritic molecules showed dissipation values of the order of 0.3×10^{-6}, which was 4−5 times lower than the one obtained for the linear polymer **L**(n = 3). The difference can be explained as reflecting the highly different degree of hydration and chain flexibility, characteristic of the two classes of macromolecules.

The combined results obtained by ellipsometry and QCM-D hence suggest that the different molecular architecture between linear and dendritic adsorbates markedly influenced the surface properties, with the dendritic adsorbates forming a relatively stiff adlayer of low hydration and low dissipation capacity, more comparable to the properties reported for oligo(ethylene glycol)-alkanethiol SAMs on gold or silver surfaces.[10,12,66] Instead, surface assemblies of the linear PEG grafts formed viscoelastic, strongly dissipating, and highly hydrated films, which displayed properties comparable to those of the widely studied PEG-based brush assemblies.

Surface Analysis by XPS. High-resolution XPS was performed on freshly cleaned TiO_2 as well as dendron and polymer-modified TiO_2 surfaces. Carbon (C1s), oxygen (O1s), nitrogen (N1s), and titanium (Ti2p) spectra were recorded and evaluated quantitatively (see exemplary spectra, Figure S5,

and Table S3 with the results of deconvolution and quantitative compositional analysis compiled in the Supporting Information). Freshly cleaned TiO_2 surface showed representative signals of Ti2p (464.6 and 458.9 eV), O1s (530.3 eV), and weak signals related to carbon- and nitrogen-containing species (respectively at 284.7 and 401.9 eV) due to minor adventitious contamination.

Upon adsorption of **D**(n = 1−3) and **L**(n = 3), significant changes of the O1s, C1s, and N1s signals were observed. The C1s signals were deconvoluted into three components on the basis of their respective binding energies: carbon next to aromatic and aliphatic carbon (C_A, 284.7 eV), carbon next to nitrogen or oxygen (C_B, 286.6 eV), and the carbonyl carbon (C_C, 288.5 eV). The O1s signals were also curve-fitted into three components: oxygen of the TiO_2 substrate (O_A, 530.2 eV), oxygen in H_2O, Ti−OH, Ti−O−C, and the carbonyl oxygen (O_B, 531.5 eV), and oxygen next to aliphatic or aromatic carbon (O_C, 533.0 eV). The N1s signal was fitted by two curves, one assigned to the amide nitrogen (N_A, 400.1 eV) and one to minor nitrogen contamination (N_B, 401.9 eV).[15,26,67] More details are provided in the Supporting Information.

Table 3 shows a compilation of relevant atomic ratios based on the intensities of the deconvoluted signals and use of appropriate sensitivity factors. The atomic ratio C_{total}/Ti is a parameter that sensitively reflects the overlayer thickness.[68] It increases with the number of catechols in the anchor group; thus the highest C_{total}/Ti values were found for the compounds **D**(n = 3) and **L**(n = 3) that are in agreement with the adlayer thicknesses determined by ellipsometry. The O_A/Ti ratio was found to be close to the theoretical value of 2.0 for all surfaces (TiO_2 contribution), while the C_B/O_C ratios (primarily reflecting contribution from ethylene glycol) were found to be in the range of 1.94−2.28, in fairly good agreement with the theoretical values of 1.93−1.96 for **D**(n = 1−3) and **L**(n = 3). The C_{total}/N_A ratios are less precise due to the low concentration of nitrogen in the polymers and correspondingly low XPS intensities. Nevertheless, the ratios C_{total}/N_A were found to decrease from **D**(n = 1) to **D**(n = 2) to **D**(n = 3) as expected for the increasing number of amide nitrogen atoms in the anchor backbone.

Table 3. Atomic Ratios of C_{total}/Ti, O_A/Ti, C_B/O_C, and C_{total}/N_A for the Bare TiO_2 Surface and the Surfaces after Assembly of the Four Macromolecules D(n = 1−3) and L(n = 3)[a]

	C_{total}/Ti	O_A/Ti	C_B/O_C	C_{total}/N_A
blank TiO_2	0.29	2.06 (2.00)	3.70	22.4
D(n = 1)	0.83	2.14 (2.00)	1.94 (1.96)	55.9 (63.0)
D(n = 2)	1.28	2.10 (2.00)	2.15 (1.94)	49.4 (45.0)
D(n = 3)	1.51	2.07 (2.00)	2.06 (1.93)	34.2 (36.0)
L(n = 3)	1.61	2.12 (2.00)	2.28 (1.94)	25.2 (37.5)

[a] Standard deviations are typically below ±10% relative. Numbers in parentheses are the calculated values based on the theoretical stoichiometry.

Stability Test. Ellipsometry was used to quantify the relative stability of the different adlayers in physiological buffer (HEPES 2) during a maximum incubation time of 12 days (288 h). Figure 5 shows the change of adlayer thickness determined by ellipsometry (in % relative to the original thickness before buffer incubation = 100%).

The stability of the adlayers strongly increased with the number of catechol groups in the anchor moiety, from **D**(n = 1) to **D**(n = 3) and **L**(n = 3). Both **D**(n = 3) and **L**(n = 3) showed an essentially irreversible binding, apart from a loss of ca. 10% of layer thickness in the early stage of the buffer incubation, likely caused by the desorption of somewhat more loosely bound molecules. An important enhancement of layer stability was observed when increasing the number of catechols in the anchor group from two to three (**D**(n = 1) to **D**(n = 2)), while a further increase of the number of catechols from three to four (**D**(n = 2) to **D**(n = 3)) resulted in a comparatively small increase of stability. These findings highlight the importance of multivalency in the binding to the substrate, which is in very close agreement with our earlier study on linear PEG-5 kDa-$DOPA_{1-3}$ on TiO_2.[15]

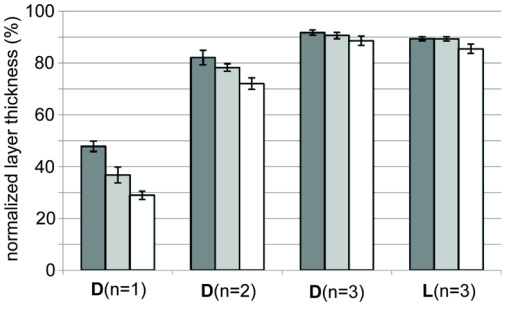

Figure 5. Test of the TiO_2 substrates coated with the four adsorbates **D**(n = 1−3) and **L**(n = 3). Remaining normalized layer thickness values, relative to the initial thickness (=100%) after 72 h (dark gray), 96 h (light gray), and 288 h (white) of incubation time in HEPES 2 buffer.

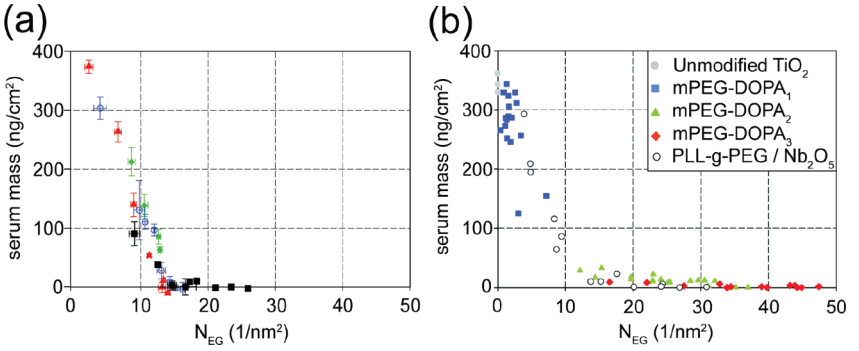

Figure 6. (a) Plot of adsorbed serum mass as a function of ethylene glycol monomer surface density (N_{EG}) for dendron and linear PEG modified surfaces (molecular weight of the PEG part; M_w = 2.5 kDa): **D**(n = 1), green ◆, **D**(n = 2), red ▲, **D**(n = 3), blue ⊙, and **L**(n = 3), ■. (b) Graph based on data from published quantitative studies on the following assembly systems: PEG-5 kDa-$DOPA_{1-3}$ (on TiO_2) and PLL-*g*-PEG (on Nb_2O_5).[15,29]

Nonfouling Surface Properties. Resistance of the four types of modified TiO_2 surfaces to nonspecific protein adsorption was tested in contact with full blood serum and quantified by ellipsometry as increase of layer thickness after 20 min of sample incubation in serum. In Figure 6a the serum adlayer thickness is plotted as a function of ethylene glycol (EG) monomer surface coverage, n_{EG} (calculated from the layer thickness values), for **D**(n = 1−3) and **L**(n = 3) assembled for different adsorption times, which correspond to different adlayer thicknesses ranging from submonolayer to saturation coverage. The amount of the adsorbed serum proteins decreased systematically with increasing adsorbate thickness, with a dependence close to the one found for other PEG systems.[29]

For both types of compounds, very low protein adsorption was found for layer thicknesses > 16 Å (Figure S7) corresponding to an ethylene glycol monomer surface density n_{EG} > 15 EG/nm^2 (Figure 6a). This is achieved, at saturation coverage, with both systems (dendritic and linear), thus representing highly nonfouling properties with adsorbed protein mass (if any) below the detection limit of the ellipsometry experiments. In situ OWLS measurements, with a lower detection limit of ∼2 ng/cm^2, confirmed this excellent nonfouling behavior (exemplary OWLS sensorgram of the adsorption of **D**(n = 3) (4.5 h) including protein adsorption test is shown in the Supporting Information, Figure S2). Figure 6b finally puts our experimental findings in the context of quantitative data of other (linear) PEG systems reported in the literature, providing further evidence for a rather universal dependence of protein resistance on EG monomer surface density.

CONCLUSIONS

The results of this work on the molecular assembly and surface properties of ethylene glycol dendron-(catechol)$_x$ conjugates on titanium oxide shed light on the importance of multivalent oligocatechol binding for both fast adsorption kinetics and high surface coverage at saturation. At least three catechols in the anchor group are required for good, essentially irreversible binding and confluency of the formed adlayers. In this comparative study of the ethylene glycol dendron-type compounds and the linear PEG analogue (both with four catechols in the anchor moiety, **D**(n = 3) and **L**(n = 3)), a number of interesting differences regarding the assembly kinetics and the resulting physicochemical properties of the surface films were established. The dendrons proved to assemble (at room temperature in the high-ionic-strength buffer) faster to form more efficiently a densely packed monolayer in comparison to its linear analogue. These differences were attributed to the smaller, less hydrated size and the much lower cloud-point (close to room temperature) of the dendron as compared to the linear analogue. In contrast to linear PEG systems where both high ionic strength and higher temperature (typically 60−70 °C) are required for fast formation of a dense brush, the dendritic compounds assemble efficiently already at room temperature.

Once a saturated monolayer is reached, both systems show excellent nonfouling properties with adsorbed protein masses below the detection limit of the two monitoring techniques used (OWLS, ellipsometry). This observation is interesting in terms of the mechanistic aspects of the nonfouling, hydrophilic polymer surfaces. While linear PEG-brush surfaces are known (and confirmed in this work) to be highly hydrated in aqueous environment (typically 80−85 wt %) with flexible chains and high dissipation values as measured with QCM-D, the dendritic adlayers were found to have rather different properties, that is, low hydration (ca. 40 wt %) and very low dissipation. Apparently, chain flexibility and high hydration are therefore not strict necessary conditions for the nonfouling character of a polymeric surface adlayer. In this respect, the dendron-type surfaces investigated here are more reminiscent of OEG-terminated alkanethiol SAMs, with the difference that the latter are known to be ordered at the molecular scale, with the type of OEG conformation very critically affecting the degree of resistance to unspecific protein adsorption.

Apart from the advantages mentioned above, dendronized surfaces with their stiffer and more confined architecture are believed to be attractive for surface (bio)engineering with regard to improved end-group (ligand) presentation. Particularly, high density of functional ligands coupled to the termini of the dendritic structure can be achieved, of interest in the light of the crucial importance of multivalent interactions for affinity or avidity in many biological processes. Therefore, the clear advantages of dendron-type assemblies versus conventional polymer brush surfaces may outweigh the increased costs and effort associated with the synthesis of functional dendritic macromolecules.

ASSOCIATED CONTENT

Supporting Information. Temperature-dependent UV−vis absorbance (at 500 nm) (cloud-point determination, Figure S1); dn/dc determination (Table S1); ellipsometry measurements of the adsorption of **D**(n = 3) and **L**(n = 3) in physiological buffer (Table S2); exemplary OWLS and QCM-D sensorgrams of the adsorption experiment of **D**(n = 3) (Figure S2, Figure S4); OWLS sensorgram of G2-COOH and PEG-2300-COOH/PEG-2300-NHS (Figure S3); XPS elemental surface composition (Table S3) and exemplary XPS high-resolution spectra of **D**(n = 3) (Figure S5); AFM images (Figure S6); adlayer-thickness dependent protein resistance (ellipsometry, Figure S7); synthesis strategy (Figure S8); purification of the final compounds (GPC elugram, Figure S9); NMR quantification of the compound concentration (Figure S10); synthetic procedures for all compounds; ^{1}H/^{13}C NMR off all compounds; and MALDI-MS spectra for the final compounds (Figures S11−53). This material is available free of charge via the Internet at http://pubs.acs.org.

AUTHOR INFORMATION

Corresponding Author
marcus.textor@mat.ethz.ch

Present Addresses
[§]Comar, S.p.A., Zimella, Italy.
[∥]Klinik für Zahnerhaltung, Präventiv- and Kinderzahnmedizin, Bern, Switzerland.
[⊥]BASF SE, Ludwigshafen, Germany.
[#]Department of Polymer Materials, Shanghai University, China.

ACKNOWLEDGMENT

We thank Stefan Hilf and Erik Reimhult for valuable discussions and Andreas Mühlebach (who passed away in 2010) for continued technical support and motivation. Financial support by the Swiss National Science Foundation (Scientific & Technological Cooperation Programme Switzerland-Russia), the

NCCR Nanosciences, Basel, and BASF Switzerland is greatly acknowledged.

REFERENCES

(1) Harris, J. M.; Zalipsky, S. *Poly(ethylene glycol): Chemistry and Biological Applications*; American Chemical Society: Washington, DC, 1997; Vol. 680.

(2) Konradi, R.; Pidhatika, B.; Mühlebach, A.; Textor, M. *Langmuir* **2008**, *24*, 613–616.

(3) Holland, N. B.; Qiu, Y.; Ruegsegger, M.; Marchant, R. E. *Nature* **1998**, *392*, 799–801.

(4) Perrino, C.; Lee, S.; Choi, S. W.; Maruyama, A.; Spencer, N. D. *Langmuir* **2008**, *24*, 8850–8856.

(5) Statz, A. R.; Meagher, R. J.; Barron, A. E.; Messersmith, P. B. *J. Am. Chem. Soc.* **2005**, *127*, 7972–7973.

(6) Jiang, S.; Cao, Z. *Adv. Mater.* **2010**, *22*, 920–932.

(7) Zhang, Z.; Chao, T.; Chen, S.; Jiang, S. *Langmuir* **2006**, *22*, 10072–10077.

(8) Coullerez, G.; Gorodyska, G.; Reimhult, E.; Textor, M.; Grandin, M. H.; Knoll, W.; Advincula, R. C. . *Functional Polymer Films*; Wiley VCH: Weinheim, 2011; Vol. 2: Characterization and Applications.

(9) Prime, K. L.; Whitesides, G. M. *J. Am. Chem. Soc.* **1993**, *115*, 10714–10721.

(10) Vanderah, D. J.; Valincius, G.; Meuse, C. W. *Langmuir* **2002**, *18*, 4674–4680.

(11) Vanderah, D. J.; La, H.; Naff, J.; Silin, V.; Rubinson, K. A. *J. Am. Chem. Soc.* **2004**, *126*, 13639–13641.

(12) Harder, P.; Grunze, M.; Dahint, R.; Whitesides, G. M.; Laibinis, P. E. *J. Phys. Chem. B* **1998**, *102*, 426–436.

(13) Gnauck, M.; Jaehne, E.; Blaettler, T.; Tosatti, S.; Textor, M.; Adler, H.-J. P. *Langmuir* **2006**, *23*, 377–381.

(14) Bozzini, S.; Petrini, P.; Tanzi, M. C.; Zürcher, S.; Tosatti, S. *Langmuir* **2009**, *26*, 6529–6534.

(15) Dalsin, J. L.; Lin, L.; Tosatti, S.; Vörös, J.; Textor, M.; Messersmith, P. B. *Langmuir* **2005**, *21*, 640–646.

(16) Malisova, B.; Tosatti, S.; Textor, M.; Gademann, K.; Zürcher, S. *Langmuir* **2010**, *26*, 4018–4026.

(17) Wach, J. Y.; Malisova, B.; Bonazzi, S.; Tosatti, S.; Textor, M.; Zürcher, S.; Gademann, K. *Chem.-Eur. J.* **2008**, *14*, 10579–10584.

(18) Zürcher, S.; Wäckerlin, D.; Bethuel, Y.; Malisova, B.; Textor, M.; Tosatti, S.; Gademann, K. *J. Am. Chem. Soc.* **2006**, *128*, 1064–1065.

(19) Waite, J. H.; Tanzer, M. L. *Science* **1981**, *212*, 1038–1040.

(20) Waite, J. H.; Tanzer, M. L. *Biochem. Biophys. Res. Commun.* **1980**, *96*, 1554–1561.

(21) Raymond, K. N.; Dertz, E. A.; Kim, S. S. *Proc. Natl. Acad. Sci. U. S.A.* **2003**, *100*, 3584–3588.

(22) Drechsel, H.; Jung, G. *J. Pept. Sci.* **1998**, *4*, 147–181.

(23) Dalsin, J. L.; Hu, B.-H.; Lee, B. P.; Messersmith, P. B. *J. Am. Chem. Soc.* **2003**, *125*, 4253–4258.

(24) Dalsin, J. L.; Messersmith, P. B. *Mater. Today* **2005**, *8*, 38–46.

(25) Amstad, E.; Gillich, T.; Bilecka, I.; Textor, M.; Reimhult, E. *Nano Lett.* **2009**, *9*, 4042–4048.

(26) Kenausis, G. L.; Vörös, J.; Elbert, D. L.; Huang, N.; Hofer, R.; Ruiz-Taylor, L.; Textor, M.; Hubbell, J. A.; Spencer, N. D. *J. Phys. Chem. B* **2000**, *104*, 3298–3309.

(27) Saxer, S.; Portmann, C.; Tosatti, S.; Gademann, K.; Zürcher, S.; Textor, M. *Macromolecules* **2009**, *43*, 1050–1060.

(28) Zoulalian, V.; Zürcher, S.; Tosatti, S.; Textor, M.; Monge, S.; Robin, J.-J. *Langmuir* **2009**, *26*, 74–82.

(29) Pasche, S.; De Paul, S. M.; Vörös, J.; Spencer, N. D.; Textor, M. *Langmuir* **2003**, *19*, 9216–9225.

(30) Kim, H. I.; Kushmerick, J. G.; Houston, J. E.; Bunker, B. C. *Langmuir* **2003**, *19*, 9271–9275.

(31) Jeon, S. I.; Lee, J. H.; Andrade, J. D.; De Gennes, P. G. *J. Colloid Interface Sci.* **1991**, *142*, 149–158.

(32) McPherson, T.; Kidane, A.; Szleifer, I.; Park, K. *Langmuir* **1998**, *14*, 176–186.

(33) Groll, J.; Amirgoulova, E. V.; Ameringer, T.; Heyes, C. D.; Röcker, C.; Nienhaus, G. U.; Möller, M. *J. Am. Chem. Soc.* **2004**, *126*, 4234–4239.

(34) Groll, J.; Ademovic, Z.; Ameringer, T.; Klee, D.; Möller, M. *Biomacromolecules* **2005**, *6*, 956–962.

(35) Wiener, E.; Brechbiel, M. W.; Brothers, H.; Magin, R. L.; Gansow, O. A.; Tomalia, D. A.; Lauterbur, P. C. *Magn. Reson. Med.* **1994**, *31*, 1–8.

(36) Kobayashi, H.; Kawamoto, S.; Jo, S.-K.; Bryant, H. L.; Brechbiel, M. W.; Star, R. A. *Bioconjugate Chem.* **2003**, *14*, 388–394.

(37) Yordanov, A. T.; Lodder, A. L.; Woller, E. K.; Cloninger, M. J.; Patronas, N.; Milenic, D.; Brechbiel, M. W. *Nano Lett.* **2002**, *2*, 595–599.

(38) Fu, Y.; Nitecki, D. E.; Maltby, D.; Simon, G. H.; Berejnoi, K.; Raatschen, H.-J.; Yeh, B. M.; Shames, D. M.; Brasch, R. C. *Bioconjugate Chem.* **2006**, *17*, 1043–1056.

(39) Liu, M.; Fréchet, J. M. J. *Pharm. Sci. Technol. Today* **1999**, *2*, 393–401.

(40) Boas, U.; Heegaard, P. M. H. *Chem. Soc. Rev.* **2004**, *33*, 43–63.

(41) Cheng, Y.; Xu, T. *Eur. J. Med. Chem.* **2008**, *43*, 2291–2297.

(42) Haensler, J.; Szoka, F. C. *Bioconjugate Chem.* **1993**, *4*, 372–379.

(43) Tang, M. X.; Redemann, C. T.; Szoka, F. C. *Bioconjugate Chem.* **1996**, *7*, 703–714.

(44) Kim, Y.-P.; Hong, M.-Y.; Shon, H. K.; Chegal, W.; Cho, H. M.; Moon, D. W.; Kim, H.-S.; Lee, T. G. *Appl. Surf. Sci.* **2008**, *255*, 1110–1112.

(45) Benhabbour, S. R.; Sheardown, H.; Adronov, A. *Macromolecules* **2008**, *41*, 4817–4823.

(46) Wyszogrodzka, M.; Haag, R. *Biomacromolecules* **2009**, *10*, 1043–1054.

(47) Li, W.; Zhang, A.; Schlüter, A. D. *Chem. Commun.* **2008**, 5523–5525.

(48) Li, W. Ph.D. Thesis, ETH: Zurich, 2010.

(49) Hilfiker, J. N.; S., R. A. *Solid State Technol.* **1998**, *41*, 101–110.

(50) Vörös, J.; Ramsden, J. J.; Csúcs, G.; Szendro, I.; De Paul, S. M.; Textor, M.; Spencer, N. D. *Biomaterials* **2002**, *23*, 3699–3710.

(51) Scofield, J. H. *J. Electron Spectrosc. Relat. Phenom.* **1976**, *8*, 129–137.

(52) Gaucher, A.; Dutot, L.; Barbeau, O.; Hamchaoui, W.; Wakselman, M.; Mazaleyrat, J.-P. *Tetrahedron: Asymmetry* **2005**, *16*, 857–864.

(53) Xu, C.; Xu, K.; Gu, H.; Zheng, R.; Liu, H.; Zhang, X.; Guo, Z.; Xu, B. *J. Am. Chem. Soc.* **2004**, *126*, 9938–9939.

(54) Yu, M.; Hwang, J.; Deming, T. J. *J. Am. Chem. Soc.* **1999**, *121*, 5825–5826.

(55) Burzio, L. A.; Waite, J. H. *Biochemistry* **2000**, *39*, 11147–11153.

(56) Lee, H.; Scherer, N. F.; Messersmith, P. B. *Proc. Natl. Acad. Sci. U.S.A.* **2006**, *103*, 12999–13003.

(57) Kingshott, P.; Thissen, H.; Griesser, H. J. *Biomaterials* **2002**, *23*, 2043–2056.

(58) Feuz, L.; Leermakers, F. A. M.; Textor, M.; Borisov, O. *Langmuir* **2008**, *24*, 7232–7244.

(59) Ramsden, J. J. *J. Stat. Phys.* **1993**, *73*, 853–877.

(60) Chen, Q.; Jia, Y.; Liu, S.; Mogilevsky, G.; Kleinhammes, A.; Wu, Y. *J. Phys. Chem. C* **2008**, *112*, 17331–17335.

(61) Li, S.-C.; Wang, J.-g.; Jacobson, P.; Gong, X. Q.; Selloni, A.; Diebold, U. *J. Am. Chem. Soc.* **2009**, *131*, 980–984.

(62) Feuz, L. Ph.D. Thesis, ETH: Zürich, 2006.

(63) Heuberger, M.; Drobek, T.; Vörös, J. *Langmuir* **2004**, *20*, 9445–9448.

(64) Pasche, S.; Textor, M.; Meagher, L.; Spencer, N. D.; Griesser, H. J. *Langmuir* **2005**, *21*, 6508–6520.

(65) Müller, M. T.; Yan, X.; Lee, S.; Perry, S. S.; Spencer, N. D. *Macromolecules* **2005**, *38*, 5706–5713.

(66) Pale-Grosdemange, C.; Simon, E. S.; Prime, K. L.; Whitesides, G. M. *J. Am. Chem. Soc.* **1991**, *113*, 12–20.

(67) Rodenstein, M.; Zürcher, S.; Tosatti, S. G. P.; Spencer, N. D. *Langmuir* **2010**, *26*, 16211–16220.

(68) Tosatti, S.; Michel, R.; Textor, M.; Spencer, N. D. *Langmuir* **2002**, *18*, 3537–3548.